Plasmonics
https://doi.org/10.1007/s11468-023-01963-1

RESEARCH

Enhancing Label-Free Biosensing With Cryogenic Temperature-Induced Plasmonic Structures

Vagif Nevruzoglu[1] · Murat Tomakin[2] · Melih Manir[1] · Selçuk Demir[3] · Fatih Şaban Beriş[4] · Arif E. Cetin[5]

Received: 22 June 2023 / Accepted: 18 July 2023

Abstract
Plasmonic nanoparticles exhibit distinct nearfield properties that offer potential advantages for label-free biosensing applications. By generating strong interactions between light and matter, these nanoparticles can be employed to detect the presence of analytes through monitoring spectral variations within the plasmonic resonances resulting from changes in the biomolecules on their surface. Various fabrication methods have been introduced in the literature to produce such particles. In this study, precise control over the shape, size, and distribution of nanoparticles is crucial to effectively excite plasmonic resonances with desirable optical properties. Traditionally, the vacuum deposition technique has been widely used to create nanoparticles with good crystalline properties and uniform particle distribution at high substrate temperatures (300 K). However, this method exhibits reduced surface or volume diffusion of particles at lower substrate temperatures, leading to a decrease in the particle size of the metal thin films. Additionally, surface homogeneity deteriorates due to the shadowing effect when dealing with thicker film coatings. To overcome these limitations, we propose a cryogenic temperature method, in which vacuum evaporation is performed at low substrate temperatures (200 K). Our method demonstrates the ability to produce nanoparticle systems with homogeneous particle size distribution and high structural quality. To evaluate the efficacy of our approach for biosensing applications, we compared two silver (Ag) nanoparticle systems prepared using the classical vacuum deposition technique (300 K) and our cryogenic temperature method (200 K) in terms of their structural and optical properties. We showed that our method enables the excitation of plasmonic resonances with narrower linewidths compared to the classical evaporation technique. Moreover, our method allows for the realization of nanoparticles with more controlled dimensions, which are homogeneously distributed over the substrate surface. This characteristic facilitates the generation of surface plasmon excitations associated with large local electromagnetic fields that extend extensively into the volume surrounding the sensing surface. Therefore, our method facilitates stronger light-matter interactions compared to the classical technique, resulting in enhanced refractive index sensitivity for label-free biosensing applications. We conducted sensing experiments using bulk solutions with different refractive indices to demonstrate the superior refractive index sensitivity of our cryogenic temperature method. Our findings indicate that our method produces plasmonic nanoparticle systems with higher refractive index sensitivities. Furthermore, when functionalizing the metal surface with protein mono- and bilayers, our method yields larger spectral shifts within the plasmonic resonances compared to the classical vacuum deposition technique. This indicates that our method has the potential to serve as a highly sensitive and label-free plasmonic biosensing platform without the need for expensive, slow, and complex fabrication techniques that require a sophisticated clean-room infrastructure. In summary, we believe that our method opens up possibilities for the development of advanced plasmonic biosensing platforms with exceptional sensitivity.

Keywords Label-free biosensing · Plasmonics · Nanoparticles · Nanofabrication · Cryogenic temperature method · Vacuum deposition technique

Introduction

Recent advancements in nanoparticle technologies have unveiled novel modalities in both near and farfield [1]. Among these, plasmonic nanoparticles have garnered

Extended author information available on the last page of the article

Published online: 25 July 2023

significant attention due to their unique physical and chemical properties that offer great potential for biosensing applications [2]. These nanoparticles enable the detection of analytes through the generation of strong light-matter interactions, leading to high sensitivity and selectivity, making them valuable tools in diagnostic and therapeutic applications [3, 4]. Plasmonic nanoparticles exhibit distinctive optical properties associated with localized surface plasmons, which are non-propagating collective oscillations of free electrons excited by incident photons. These interactions result in the formation of standing field patterns around the nanoparticles. The optical characteristics of these surface electromagnetic waves can be statically tuned by altering the shape and size of the nanoparticles [5], or dynamically manipulated by integrating them with phase-change materials [6]. By confining light at the nanoscale, plasmonic nanoparticles exhibit pronounced absorption and scattering properties, thereby amplifying surface plasmon resonance (SPR) and spectroscopic signals [7], as well as enabling surface-enhanced Raman scattering [8]. Moreover, the interaction between metallic nanoparticles and fluorophores leads to enhanced fluorescence signals [9]. Additionally, the aggregation of plasmonic nanoparticles can induce distinct color variations, which can be exploited for naked-eye detection of analytes [10].

The scientific literature presents various fabrication methods for the production of metallic nanoparticles, including the green method [11], successive ionic layer deposition [12], sputtering [13], and physical vapor deposition [14]. Achieving optimal plasmon resonance scattering requires precise control over the size and shape of the nanoparticles, which often poses a challenge [15]. Consequently, it is imperative to explore novel techniques that can yield metallic nanoparticles with uniform sizes, well-defined shapes, and extensive coverage over large areas. The classical vacuum deposition technique, commonly employed at high substrate temperatures (>300 K), is a well-established method for generating crystalline films with uniform properties. The film formation process in this technique is elucidated by the structural zone model [16]. According to this model, particle diffusion from the vapor medium, either at the surface or within the volume, decreases as the substrate temperature decreases. As a result, the particle size of the metal thin films decreases as the substrate temperature is reduced. However, at low temperatures (e.g., $T_s/T_m < 0.2$, where T_s represents the substrate temperature and T_m denotes the melting temperature of the source material), the particles exhibit a columnar structure within the structural zone model. Furthermore, with the increasing film thickness, the surface homogeneity deteriorates due to the shadowing effect [17]. On the contrary, the film formation process at cryogenic temperatures (<300 K), known as the cryogenic temperature method or cold substrate method, is elucidated by the soliton model [18]. The growth mechanism in the soliton model ensures that only particles of critical size adhere to the substrate, while the remaining particles depart without energy loss [19]. This mechanism results in a homogeneous distribution of particle sizes and high structural quality at cryogenic temperatures [20].

This article presents a comparative analysis of two silver (Ag) nanoparticle systems fabricated using vacuum evaporation at different substrate temperatures: 300 K (classical vacuum deposition technique) and 200 K (cryogenic temperature method). Our investigation focuses on evaluating the structural and optical properties of these systems for potential biosensing applications. Our findings demonstrate that the cryogenic temperature method enables the excitation of plasmonic resonances with narrower linewidths in comparison to the classical vacuum deposition technique. By employing the cryogenic temperature method, we achieve metallic nanoparticles with enhanced control over their size and dimensions. Consequently, the resulting nanoparticle systems exhibit larger and more accessible local electromagnetic fields in the proximity of the sensing surface, crucial for facilitating strong light-matter interactions. Moreover, our Ag nanoparticle system produced using the cryogenic temperature method demonstrates heightened refractive index sensitivities, surpassing those achieved through the classical vacuum deposition technique. This enhanced sensitivity is highly advantageous for label-free biosensing applications. In label-free biosensing experiments involving protein mono- and bilayers, our cryogenic temperature method yields larger spectral shifts within the plasmonic resonances supported by the nanoparticle systems. This superior performance is attributed to the improved sensing properties inherent to our method. Overall, our study highlights the significant advantages of the cryogenic temperature method in fabricating plasmonic nanoparticle systems for biosensing applications, demonstrating its ability to achieve narrower linewidths, increased refractive index sensitivities, and larger spectral shifts within plasmonic resonances.

Comparison Between Cryogenic Temperature Method and Classical Vacuum Deposition

To elucidate the advantages of our cryogenic temperature method over the classical vacuum deposition technique in the context of biosensing applications, we fabricated plasmonic chips composed of silver (Ag) nanoparticles. The Ag nanoparticles were deposited onto glass substrates using vacuum evaporation at temperatures of 200 K and 300 K. For this purpose, a high-purity Ag wire (99.9% purity, 1-mm diameter, Alfa Aesar) was utilized as the source material. Initially, 0.1 g of the Ag wire was

placed within a tungsten boat source heater (88.9 mm L × 12.7 mm W × 3.175 mm deep, inverted top-hat dimple, Kurt J. Lesker). The glass substrates (20 mm L × 10 mm W × 1 mm thickness) were mounted onto a removable substrate holder with a diameter of 70 mm. During the vacuum process, the base pressure was monitored until it reached a value of 8.0×10^4 Pa. At this point, a flow of liquid nitrogen was directed through a copper pipe with an 8-mm diameter to cool the glass substrate. Figure 1A presents a three-dimensional representation of the vacuum chamber and the evaporation apparatus. Both the liquid nitrogen flow and the substrate temperature were manually controlled. Once the substrate temperature reached the desired value, the tungsten boat was electrically powered, leading to the evaporation of the Ag source material (Fig. 1B-I). Following the establishment of the ideal Ag vapor environment, the shutter was opened, enabling the Ag nanoparticles to deposit onto the glass substrate (Fig. 1B-II). A thin film layer composed of Ag nanoparticles was formed on the glass substrate over a period of 15 s with the shutter held open. The coating process was finalized by closing the shutter (Fig. 1B-III).

The crystal structure of Ag thin films was analyzed using powder X-ray diffraction (PXRD) on a Rigaku SmartLab diffractometer with CuK radiation (1.5408 Å). The investigation covered a range of 30 to 90° (2θ) at room temperature. PXRD patterns (Fig. 1C, D) effectively illustrate the structural characteristics of Ag thin films prepared at 300 K and 200 K, respectively. Both films exhibit a polycrystalline cubic structure, featuring reflection planes of (111), (200), (220), and (311). The preferred orientation in Ag films is the (111) reflection plane. Ag thin films deposited on amorphous surfaces tend to exhibit (111) orientation due to the reduced surface

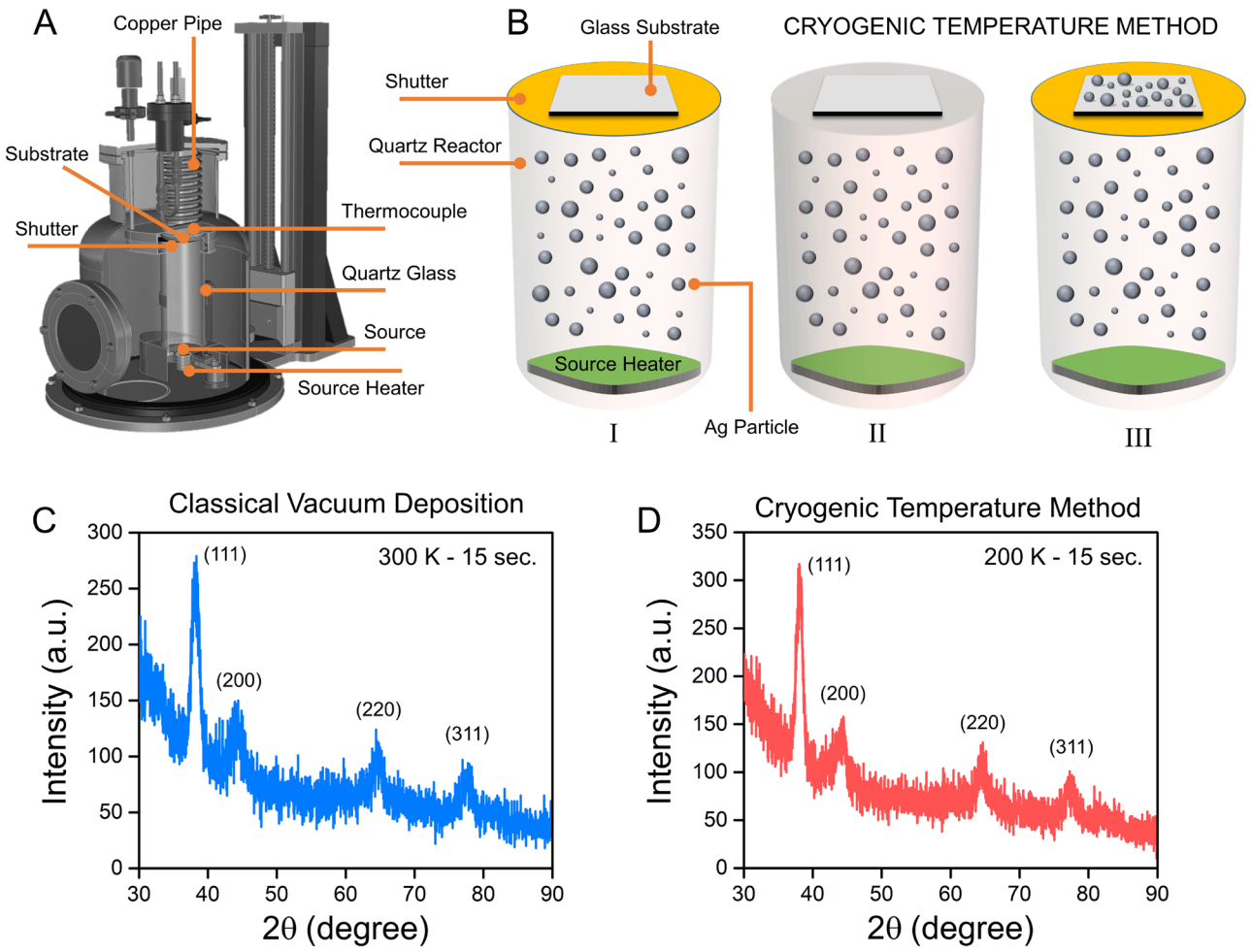

Fig. 1 **A** Three-dimensional representation of the vacuum chamber and evaporation apparatus. **B** Depiction of the thin film formation process employing the cryogenic temperature method. Powder X-ray diffraction (PXRD) patterns illustrating the structural characteristics of Ag nanoparticle-based plasmonic chips prepared at substrate temperatures of **C** 300 K (using the classical vacuum deposition technique) and **D** 200 K (employing the cryogenic temperature method)

energy [21]. However, we observed that there was no significant change in the peak intensities depending on the deposition temperature.

Figure 2A presents a schematic illustration of Ag nanoparticles grown on a glass substrate. The farfield characteristics of the two nanoparticle systems were evaluated using visible-range spectroscopy (Ocean Insight HR4000). The absorbance spectra of the nanoparticles prepared using the classical vacuum deposition technique (blue curve) and the cryogenic temperature method (red curve) are shown in Fig. 2B. Both systems exhibit plasmonic resonance at similar wavelengths, ~450.2 nm (300 K) and 444.8 nm (200 K). Notably, the nanoparticle system fabricated with the cryogenic temperature method displays a narrower optical response compared to the classical vacuum deposition technique, with bandwidths of 90 nm (300 K) and 78 nm (200 K), respectively.

In order to examine the surface morphology and particle size of Ag thin films, we employed field emission scanning electron microscopy (FE-SEM, Zeiss Sigma 300). FE-SEM measurements were conducted under high vacuum conditions using a secondary electron detector, with an accelerating voltage of 5 kV and a working distance of 4.4 mm. The FE-SEM images in Fig. 2C (300 K) and D (200 K) reveal that the growth of particle islands, following the classical vacuum deposition mechanism, results in the formation of a crystal structure comprising nano-islands of varying sizes. In contrast, the soliton growth mechanism, employed through cryogenic temperature methods, yields a crystal structure composed of clusters with similar dimensions. Here, a small number of large and elongated grains could be also observed in the FE-SEM images for 200 K. The interaction between dislocations at the interface between the substrate and film gives rise to distinct soliton waves, leading to the formation of Ag nanoparticles with diverse sizes and shapes [20]. This mechanism can exert dominance depending on the substrate temperature, causing non-homogeneity in grain size even at cryogenic temperatures. Similar findings were noted for Ag nanoparticles grown on Si substrates, where the grain structure of the Ag thin film on the Si substrate becomes spherical, small, and homogeneous as the substrate temperature is reduced to 200 K [22]. However, further decrease in the substrate temperature results in an increase in grain size and a deterioration in the uniformity of grain size distribution. To determine the nanoparticle size in the thin film, we conducted image analyses of the FE-SEM images using ImageJ software. The histogram shown in Fig. 2E, F represents the Ag nanoparticles prepared at 300 K and 200 K, respectively. The average

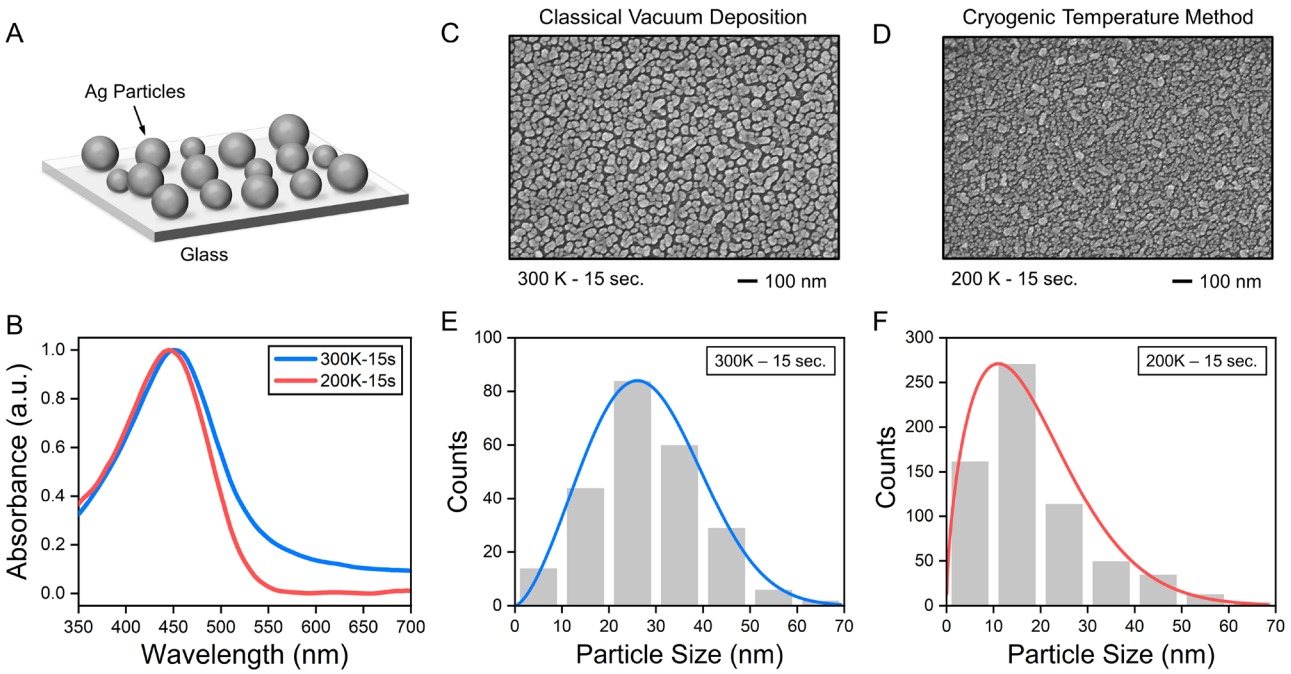

Fig. 2 **A** Schematic illustration of the Ag nanoparticle-based plasmonic substrate. **B** Absorbance spectra of the nanoparticle systems fabricated using the classical vacuum deposition technique (blue curve: 300 K – 15 s) and the cryogenic temperature method (red curve: 200 K – 15 s). Field emission scanning electron microscopy (FE-SEM) images of the nanoparticles grown on a glass substrate at **C** 300 K and **D** 200 K for 15 s deposition. Size distribution of Ag nanoparticles for the coating temperatures of **E** 300 K (vacuum deposition technique) and **F** 200 K (cryogenic temperature method)

particle size was determined as 26.79 ± 0.73 nm (300 K) and 13.35 ± 0.50 nm (200 K).

FDTD Nearfield Calculations of Nanoparticle Systems

In order to demonstrate the advantages of our cryogenic temperature method over classical vacuum deposition, we conducted FDTD simulations on two nanoparticle systems. The nanoparticle systems were modeled based on the Weibull Distribution ($f(x) = \gamma x^{(\gamma-1)} e^{-(x^{\gamma})}$, where γ is the shape parameter with particle sizes ranging from 5 to 55 nm for 300 K - 15 s (Fig. 2E, blue line) and 200 K - 15 s (Fig. 2F, red line). As depicted in Fig. 3, we employed an unpolarized light source incident normal to the nanoparticle surface. Perfectly matched layer boundary conditions were applied along all axes, and a mesh size of 0.2 nm was chosen for the simulations. Figure 3A, B illustrate the distribution of electric field magnitude (|E|) calculated in a 300 nm × 300 nm area on the *xy*-plane at the plasmonic resonance supported by each nanoparticle system. The nearfield distributions reveal that in the cryogenic temperature method, local electromagnetic fields with high intensities are more uniformly distributed over a larger area compared to the classical vacuum deposition technique. This characteristic is particularly crucial for biosensing applications, as it enhances light-matter interactions. Moreover, the increased number of hotspots with intense local electromagnetic fields indicates stronger interactions between nanoparticles. These interactions also lead to narrower absorbance signals in the nanoparticle system fabricated using the cryogenic temperature method, as opposed to the classical vacuum deposition technique.

To quantify this enhancement, we calculated the integral of the electric field magnitude to determine the total available electromagnetic fields with high intensities. In the subsequent section, we conducted label-free biosensing experiments using protein bilayers consisting of protein A/G and protein IgG, with a total thickness of approximately 7.9 nm determined by ellipsometry measurements [23]. We computed the sum of electromagnetic fields within a volume of 7.9 nm height, with the surface of the plasmonic chip as the baseline. Our results demonstrate that the cryogenic temperature method supports 1.83 times larger available electromagnetic fields compared to the classical vacuum deposition technique, which is critical for label-free biosensing experiments based on refractive index variations.

Label-Free Experiments With Nanoparticle Systems

In order to evaluate the impact of our fabrication technique on the sensing capabilities of particle-based plasmonic substrates, we conducted sensing experiments using different refractive indices of bulk solutions, such as DI-water ($n = 1.33$), acetone ($n = 1.35$), ethanol ($n = 1.36$), and isopropanol ($n = 1.37$). Figure 4A illustrates the spectral variations of the plasmonic resonance based on the refractive index of the bulk solutions for the cryogenic temperature method (red line) and the vacuum deposition technique (blue line). We observed a linear relationship between the spectral position of the plasmonic resonance (λ) and the refractive index of the bulk solutions (n), represented by $\lambda = 508.57n + 19.8$ (vacuum deposition technique) and $\lambda = 551.430n + 18.3$ (cryogenic temperature method). Importantly, our cryogenic temperature method exhibited higher refractive index sensitivity ($S = \Delta\lambda/\Delta n$) compared to the vacuum deposition technique, with values of S (200 K) = 551.430 and S (300 K) = 508.57. This enhanced sensitivity can be attributed to the larger number of available local electromagnetic fields in our method compared to the classical technique. As

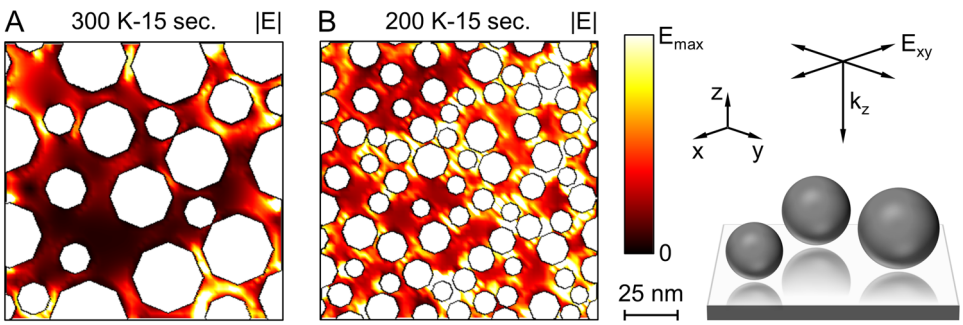

Fig. 3 Electric field distributions calculated at the plasmonic resonances supported by the nanoparticle systems modeled using **A** the classical vacuum deposition technique (300 K - 15 s) and **B** the cryogenic temperature method (200 K - 15 s). The schematic illustration depicts the Ag nanoparticle system, along with the propagation and polarization directions of the illuminating light source

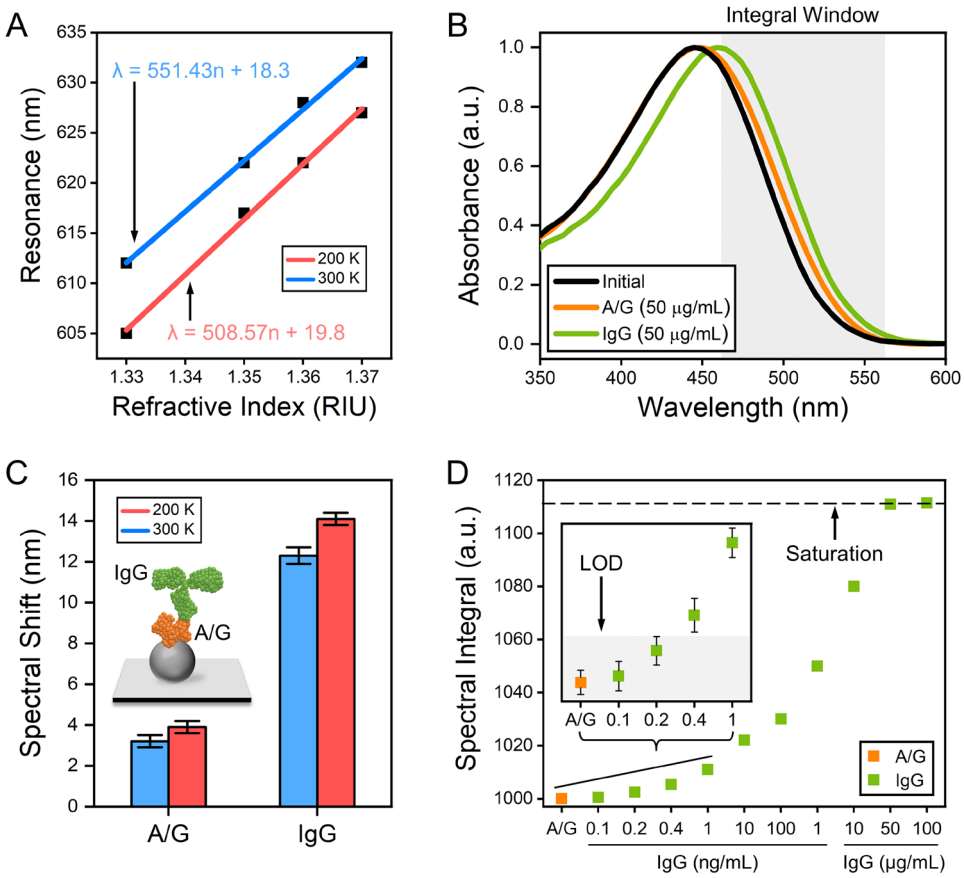

Fig. 4 **A** Spectral position of the plasmonic resonance under various refractive indices of bulk solutions for the nanoparticle systems fabricated using the vacuum deposition technique (blue line) and the cryogenic temperature method (red line). The refractive index sensitivity is determined from the linear fit to the experimental data (represented by black square dots). **B** Absorbance spectra of the nanoparticle system fabricated through the cryogenic temperature method: initial response (black line), attachment of 50 μg/mL protein A/G (orange line), and attachment of 50 μg/mL protein IgG (green line). The gray area represents the spectral window used for spectral integral calculations. **C** Spectral shifts observed within the plasmonic resonance supported by the nanoparticle systems upon the binding of protein A/G and protein IgG using the vacuum deposition technique (blue column) and the cryogenic temperature method (red column). Error bars represent twice the standard deviation of five independent experiments. The figure inset illustrates the schematic of analyte binding on the Ag nanoparticle surface. **D** Spectral integral values calculated for 50 μg/mL protein A/G (orange square) and different protein IgG concentrations ranging from 0.1 ng/mL to 100 μg/mL (green squares). The limit-of-detection (LOD) of the nanoparticle system is highlighted in gray. The maximum spectral integral value, corresponding to surface saturation, is indicated by the black dashed line

an additional note, for bulk solutions with different refractive indices, the spectral shape of the plasmonic resonance supported by both nanofabrication systems exhibits negligible variations (not shown here). Furthermore, the literature shows that plasmonic resonances at longer wavelengths provide superior sensitivities compared to their counterparts at shorter wavelengths [24]. As shown before, the cryogenic temperature method yields a nanoparticle system that supports a plasmonic resonance at wavelengths ~5 nm shorter compared to the one supported by the vacuum deposition technique. Despite the shorter wavelength of the plasmonic resonance supported by the cryogenic temperature method, it still achieves better sensitivity. This outcome is attributed to the larger and more accessible local electromagnetic fields facilitated by the nanoparticle system realized through the cryogenic temperature method. The performance of plasmonic sensors can be effectively assessed through the use of the figure of merit (FOM). The FOM is determined by calculating the ratio between the sensitivity (S) and the full width at half maximum (FWHM) of the plasmonic features, represented as FOM = S/FWHM [25]. In comparison, the cryogenic temperature method demonstrates superior FOM values when compared to the vacuum deposition technique, which is attributed to the cryogenic temperature method exhibiting higher sensitivities and exciting plasmonic resonances with sharper bandwidths. Here, the cryogenic temperature method achieves an FOM of 6.49, whereas the vacuum deposition technique supports an FOM of 5.21.

To further demonstrate the advantages of our fabrication technique over the classical method in biosensing

applications, we conducted label-free biosensing experiments using protein mono- and bilayers. Figure 4B displays the absorbance spectrum of the nanoparticle system realized through the cryogenic temperature method. In these experiments, we initially immobilized protein A/G on the particle surface, followed by functionalizing the A/G-covered surface with protein IgG. We utilized purified protein samples that were dissolved in PBS (phosphate-buffered saline). Following each functionalization step, the sensing surface was rinsed with PBS to eliminate any unbound proteins from the surface. Protein A/G is a fusion protein that contains binding sites for both protein A and protein G. This protein binds to the Ag particle surface through physisorption, which has a high affinity for the Fc region of protein IgG. Protein IgG then binds to the surface through its Fc region. The initial plasmonic resonance (black line) shifted by ~4.1 nm and ~14.2 nm upon the addition of 50 µg/mL protein A/G (orange line) and 50 µg/mL protein IgG (green line), respectively. Figure 4C illustrates the spectral shifts within the plasmonic response supported by the nanoparticle systems fabricated using the classical vacuum deposition technique (blue column) and the cryogenic temperature method (red column). The columns represent the averages of five different experiments, while the error bars indicate twice the standard deviation. The presence of 50 µg/mL protein A/G resulted in average spectral shifts of ~3.2 nm and ~3.9 nm for the vacuum deposition technique and cryogenic temperature method, respectively. Functionalizing the nanoparticle surface with 50 µg/mL protein IgG led to a total shift of 12.3 nm for the vacuum deposition technique and 14.1 nm for the cryogenic temperature method. These relatively high protein concentrations were used to saturate the plasmonic chip surface, enabling a reliable comparison of the sensing abilities between the two nanoparticle systems. These results clearly demonstrate that our fabrication method further enhances the sensing capabilities of the nanoparticle system by generating strong localized surface plasmons accessible to analytes in the vicinity of the sensing surface.

To determine the limit-of-detection of the nanoparticle system realized using the cryogenic temperature method, we conducted a characterization study with various protein IgG concentrations. To generate a spectral sensing signal at low analyte concentrations, we employed a spectral integral method [26]. This method involves calculating the integral of the absorbance spectrum within a 100-nm-wide spectral window, highlighted in gray in Fig. 4B. By using this approach, we were able to capture multiple spectral shifts resulting from analyte attachments, leading to improved refractive index sensitivities compared to monitoring a single spectral data point such as the absorbance peak or dip. Figure 4D presents the spectral integral values obtained for different IgG concentrations ranging from 0.1 ng/mL to 100 µg/mL (green squares), along with the value for 50 µg/mL protein A/G (orange square). The high concentration of protein A/G, which serves as a capturing ligand, was used to effectively capture protein IgG on the sensing surface, ensuring a reliable comparison across different IgG concentrations. As expected, higher IgG concentrations resulted in a spectral shift within the absorbance resonance towards longer wavelengths, aligning it better with the integral window, which increases the spectral integral value. In the figure, the squares represent the mean values of the spectral integral values determined for each protein IgG concentration, and the error bars indicate twice the standard deviation from five independent experiments. As depicted, the spectral integral values reach a plateau (represented by the black dashed line) after reaching a concentration of 50 µg/mL protein IgG, indicating surface saturation with the targeted analytes. The inset in Fig. 4D zooms in on the concentration range between 0.1 and 1 ng/mL. In this range, the spectral integral values associated with 50 µg/mL protein A/G, 0.1 ng/mL, and 0.2 ng/mL protein IgG cannot be reliably distinguished from each other. However, the spectral integral value corresponding to 0.4 ng/mL protein IgG demonstrates a significant change, indicating the minimum detectable IgG concentration using the nanoparticle system realized with the cryogenic temperature method is 0.4 ng/mL (highlighted in gray in the figure).

Conclusion

In conclusion, we have introduced a cryogenic temperature method for film formation, specifically at 200 K, which offers superior control over the shape, size, and distribution of metallic nanoparticles compared to the classical vacuum deposition technique employed at higher substrate temperatures, e.g., 300 K. Our method enables the fabrication of nanoparticles that support plasmonic resonances with more distinct spectral characteristics compared to those achieved through the conventional evaporation technique. Furthermore, the nanoparticles produced using our cryogenic temperature method exhibit enhanced ability to excite large local electromagnetic waves that are accessible to the surrounding medium due to the improved control over nanoparticle size and distribution over a larger area. Consequently, our cryogenic temperature method yields greater refractive index sensitivities in comparison to the classical vacuum deposition technique, which was demonstrated through refractive index experiments conducted with bulk solutions. Moreover, our method achieved larger spectral shifts within the plasmonic resonances during label-free experiments conducted with protein mono- and bilayers, thanks to its heightened sensitivity compared to the classical vacuum deposition technique. By offering a robust control mechanism for the physical properties of

nanoparticles, we believe our innovative vacuum evaporation method, which allows film formation at low substrate temperatures, holds the potential to realize plasmonic chips with formidable sensing capabilities without the need for complex nanofabrication processes.

Author Contribution V.N., M.T., M.M., S.D., and F.S.B. were responsible for the fabrication and characterization of the nanoparticle-based chips. A.E.C. conducted FDTD simulations, performed label-free biosensing experiments, and led the research project.

Data Availability Data for this study is accessible upon request.

Declarations

Competing Interests V.N., M.T., and F.S.B. have a granted patent (TR2018/11733B) for the presented cryogenic temperature method.

References

1. Liu J, He H, Xiao D et al (2018) Recent advances of plasmonic nanoparticles and their applications. Materials (Basel) 11:1833. https://doi.org/10.3390/ma11101833
2. Su H, Li S, Jin Y et al (2017) Nanomaterial-based biosensors for biological detections. Adv Heal Care Technol 3:19–29. https://doi.org/10.2147/AHCT.S94025
3. Martín-Gracia B, Martín-Barreiro A, Cuestas-Ayllón C et al (2020) Nanoparticle-based biosensors for detection of extracellular vesicles in liquid biopsies. J Mater Chem B 8:6710–6738. https://doi.org/10.1039/D0TB00861C
4. Dykman L, Khlebtsov N (2012) Gold nanoparticles in biomedical applications: recent advances and perspectives. Chem Soc Rev 41:2256–2282. https://doi.org/10.1039/C1CS15166E
5. Loiseau A, Asila V, Boitel-Aullen G et al (2019) Silver-based plasmonic nanoparticles for and their use in biosensing. Biosensors 9:78. https://doi.org/10.3390/bios9020078
6. Pawlak M, Bagiński M, Llombart P et al (2022) Tuneable helices of plasmonic nanoparticles using liquid crystal templates: molecular dynamics investigation of an unusual odd–even effect in liquid crystalline dimers. Chem Commun 58:7364–7367. https://doi.org/10.1039/D2CC00560C
7. Jana J, Ganguly M, Pal T (2016) Enlightening surface plasmon resonance effect of metal nanoparticles for practical spectroscopic application. RSC Adv 6:86174–86211. https://doi.org/10.1039/C6RA14173K
8. Hu Y, Cheng H, Zhao X et al (2017) Surface-enhanced raman scattering active gold nanoparticles with enzyme-mimicking activities for measuring glucose and lactate in living tissues. ACS Nano 11:5558–5566. https://doi.org/10.1021/acsnano.7b00905
9. Reis DS, de Oliveira VL, Silva ML et al (2021) Gold nanoparticles enhance fluorescence signals by flow cytometry at low antibody concentrations. J Mater Chem B 9:1414–1423. https://doi.org/10.1039/D0TB02309D
10. Moitra P, Alafeef M, Dighe K et al (2020) Selective naked-eye detection of SARS-CoV-2 mediated by N gene targeted antisense oligonucleotide capped plasmonic nanoparticles. ACS Nano 14:7617–7627. https://doi.org/10.1021/acsnano.0c03822
11. Maťátková O, Michailidu J, Miškovská A et al (2022) Antimicrobial properties and applications of metal nanoparticles biosynthesized by green methods. Biotechnol Adv 58:107905. https://doi.org/10.1016/j.biotechadv.2022.107905
12. Kaneva MV, Gulina LB, Tolstoy VP (2022) Pt nanoparticles synthesized by successive ionic layers deposition method and their electrocatalytic properties in hydrogen evolution reaction during water splitting in the acidic medium. J Alloys Compd 901:163640. https://doi.org/10.1016/j.jallcom.2022.163640
13. Sriubas M, Bockute K, Palevicius P et al (2022) Antibacterial activity of silver and gold particles formed on titania thin films. Nanomaterials 12:1190. https://doi.org/10.3390/nano12071190
14. Lebioda M, Korzeniewska E (2022) Atypical properties of a thin silver layer deposited on a composite textile substrate. Materials (Basel) 15:1814. https://doi.org/10.3390/ma15051814
15. Mendes MJ, Morawiec S, Simone F et al (2014) Colloidal plasmonic back reflectors for light trapping in solar cells. Nanoscale 6:4796–4805. https://doi.org/10.1039/C3NR06768H
16. Messier R, Giri AP, Roy RA (1984) Revised structure zone model for thin film physical structure. J Vac Sci Technol A: Vac Surf Films 2:500–503. https://doi.org/10.1116/1.572604
17. Mukherjee S, Gall D (2013) Structure zone model for extreme shadowing conditions. Thin Solid Films 527:158–163. https://doi.org/10.1016/j.tsf.2012.11.007
18. Yeşil Duymuş Z, Nevruzoğlu V, Ateş SM et al (2020) Use of the cold substrate method for biomaterials: the structural and biological properties of the Ag layers deposited on Ti-6Al-4V. J Mater Eng Perform 29:2909–2919. https://doi.org/10.1007/s11665-020-04834-6
19. Altuntas M, Beris FS, Nevruzoglu V et al (2023) Deposition and characterization of the Ag nanoparticles on absorbable surgical sutures at the cryogenic temperatures. Appl Phys A 129:128. https://doi.org/10.1007/s00339-023-06406-6
20. Yüzüak GD, Yüzüak E, Nevruzoğlu V, Dinçer İ (2019) Role of low substrate temperature deposition on Co–Fe thin films. Appl Phys A 125:794. https://doi.org/10.1007/s00339-019-3096-5
21. Zoo Y, Alford TL (2007) Comparison of preferred orientation and stress in silver thin films on different substrates using x-ray diffraction. J Appl Phys 101:033505. https://doi.org/10.1063/1.2401654
22. Nevruzoğlu V, Bal Altuntaş D, Tomakin M (2020) Cold substrate method to prepare plasmonic Ag nanoparticle: deposition, characterization, application in solar cell. Appl Phys A 126:255. https://doi.org/10.1007/s00339-020-3433-8
23. Wu C, Khanikaev AB, Adato R et al (2012) Fano-resonant asymmetric metamaterials for ultrasensitive spectroscopy and identification of molecular monolayers. Nat Mater 11:69–75. https://doi.org/10.1038/nmat3161
24. White IM, Fan X (2008) On the performance quantification of resonant refractive index sensors. Opt Express 16:1020. https://doi.org/10.1364/OE.16.001020
25. Offermans P, Schaafsma MC, Rodriguez SRK et al (2011) Universal scaling of the figure of merit of plasmonic sensors. ACS Nano 5:5151–5157. https://doi.org/10.1021/nn201227b
26. Cetin AE, Etezadi D, Galarreta BC et al (2015) Plasmonic nanohole arrays on a robust hybrid substrate for highly sensitive label-free biosensing. ACS Photonics 2:1167–1174. https://doi.org/10.1021/acsphotonics.5b00242

Authors and Affiliations

Vagif Nevruzoglu[1] · Murat Tomakin[2] · Melih Manir[1] · Selçuk Demir[3] · Fatih Şaban Beriş[4] · Arif E. Cetin[5]

✉ Arif E. Cetin
arifengin.cetin@ibg.edu.tr

[1] Department of Energy Systems Engineering, Recep Tayyip Erdogan University, Rize 53100, Turkey

[2] Department of Physics, Recep Tayyip Erdogan University, Rize 53100, Turkey

[3] Department of Chemistry, Recep Tayyip Erdogan University, Rize 53100, Turkey

[4] Department of Biology, Recep Tayyip Erdogan University, Rize 53100, Turkey

[5] Izmir Biomedicine and Genome Center, Balcova, Izmir 35340, Turkey